J|A|C|S
A R T I C L E S

Adsorptive and Acidic Properties, Reversible Lattice Oxygen Evolution, and Catalytic Mechanism of Cryptomelane-Type Manganese Oxides as Oxidation Catalysts

Jian Luo,*,[†,‡] Qiuhua Zhang,[§] Javier Garcia-Martinez,[‖] and Steven L. Suib[†,§,⊥]

U-60, Department of Chemistry, Department of Chemical Engineering, and Institute of Materials Science, University of Connecticut, Storrs, Connecticut 06269-3060, KL Chemical Technologies, Inc., Peru, Illinois 61354, and Inorganic Chemistry Department, University of Alicante, Carretera San Vicente s/n, E-03690 Alicante, Spain

Received October 7, 2007; E-mail: Jian.luo@klchemtech.com

Abstract: Cryptomelane-type manganese oxides have been synthesized, characterized, and tested in the total oxidation of volatile organic compounds and CO oxidation. The structural, compositional, morphological, acid–base, physisorptive–chemisorptive, and thermal stability properties (especially the reversible evolution of lattice oxygen) have been studied in detail using ICP-AES (inductively coupled plasma-atomic emission spectroscopy), HRSEM (high-resolution scanning electronic microscope), XRD (X-ray diffraction), IR (infrared) and adsorbate-IR, N_2 and CO_2 physisorption at 77 and 273 K, respectively, TPD-MS (temperature-programmed decomposition–mass spectroscopy), and TGA-DSC (thermogravimetric analysis–differential scanning calorimetry) techniques. Kinetic and mechanistic studies for the catalytic function have been conducted and related to the characterization results. Cryptomelane has shown to be highly microporous, by using CO_2 physisorption, and highly hydrophobic, possessing both Brönsted and Lewis acid sites. A part of the lattice oxygen atoms can be reversibly removed from the framework and recovered at elevated temperature without changing the framework structure. These lattice oxygen atoms can react with CO even at room temperature and are active sites for the oxidation of benzene. The consumed lattice oxygen atoms are replenished by gaseous oxygen to complete a catalytic cycle. The ease of reversible evolution of lattice oxygen, together with the high porosity, hydrophobicity, and acidity, leads to the excellent oxidation properties of OMS-2.

1. Introduction

Cryptomelane is a type of manganese oxide composed of 2×2 edge-shared MnO_6 octahedra chains, which are corner connected to form one-dimensional tunnels of ca. 4.7×4.7 Å.[1,2] In recent years we have developed several processes to prepare the cryptomelane-type and many other kinds of manganese oxides and tested them in oxidation reactions and other applications. The synthetic counterpart of cryptomelane is known as octahedral molecular sieve OMS-2 (Figure 1).[2–4] These manganese oxides have potential and current uses as ion-exchange materials, battery materials, radioactive waste immobilization materials, and catalytic materials.[5,6,8–15] Some work

has been published on manganese oxides in oxidation catalysts for CO oxidation, oxidation of allylic alcohols to aldehydes or ketones, oxidative dehydrogenation of hexane to hexene, and total oxidation of low alkanes, as well as decomposition of H_2O_2 and NO_x.[8–15] However, little has been reported on the catalytic characterization/mechanism such as sorptive properties, acidic properties, and mobility and roles of lattice oxygen atoms.

Although structurally OMS-2 is microporous (with pore size of around 4.7×4.7 Å), regular nitrogen adsorption experiments result in very little micropore volume[28–30] due to the diffusion

† Department of Chemistry, University of Connecticut.
‡ KL Chemical Technologies, Inc.
§ Institute of Materials Science, University of Connecticut.
‖ Inorganic Chemistry Department, University of Alicante.
⊥ Department of Chemical Engineering, University of Connecticut.

(1) Post, J. E.; Von Dreele, R. B.; Buseck, P. R. *Acta Crystallogr.* **1982**, *B38*, 1056−1064.
(2) DeGuzman, R. N.; Shen, Y. F.; Neth, E. J.; Suib, S. L.; O'Young, C. L.; Levine, S.; Newman, J. M. *Chem. Mater.* **1994**, *6*, 815−821.
(3) Duan, N.; Suib, S. L.; O'Young, C. L. *J. Chem. Soc., Chem. Commun.* **1995**, 1367−1368.
(4) Ching, S.; Roark, J. L.; Duan, N.; Suib, S. L. *Chem. Mater.* **1997**, *9*, 750−754.
(5) Giovanoli, R.; Balmer, B. *Chimia* **1981**, *35*, 53−55.
(6) Golden, D. C.; Dixon, J. B.; Chen, C. C. *Clays Clay Miner.* **1986**, *34*, 511−520.
(7) Potter, R. M.; Rossman, G. R. *Am. Miner.* **1979**, *64*, 1199−1218.
(8) Rask, J. H.; Buseck, P. R. *Am. Miner.* **1986**, *71*, 805−814.
(9) Shen, Y. F.; Suib, S. L.; O'Young, C. L. *J. Catal.* **1996**, *161*, 115−122.
(10) Wang, J. Y.; Xia, G. G.; Yin, Y. G.; Suib, S. L.; O'Young, C. L. *J. Catal.* **1998**, *176*, 275−284.
(11) Wong, S. T.; Cheng, S. *Inorg. Chem.* **1992**, *31*, 1165−1172.
(12) Suib, S. L. *Stud. Surf. Sci. Catal.* **1996**, *102*, 47−74.
(13) Yoshizawa, K.; Shiyota, Y.; Yamabe, T. *J. Am. Chem. Soc.* **1998**, *120*, 564−572.
(14) Yamashita, T.; Vannice, A. *J. Catal.* **1996**, *163*, 158−168.
(15) Weisz, P. B. *J. Catal.* **1968**, *10*, 407−408.
(16) Auguer, G.; Landolt, R. USP 3702886, 1972.
(17) Kokotailo, G. T.; Lawton, S. L.; Olson, D. H. *Nature* **1978**, *272*, 437−438.
(18) Luo, J.; Suib, S. L. *J. Phys. Chem. B* **1997**, *101*, 10403−10413.
(19) Shen, Y. F.; Zerger, R. P.; DeGuzman, R. N.; Suib, S. L.; McCurdy, L.; Potter, D. I.; O'Young, C. L. *Science* **1993**, *260*, 511−515.
(20) Parry, E. P. *J. Catal.* **1963**, *2*, 371−376.
(21) Martínez, J. G. D.; Amorós, C.; Solano, A. L. *Stud. Surf. Sci. Catal.* **2000**, *128*, 485−494.

(a) OL-1

(b) OMS-2

⊠ MnO$_6$ Unit

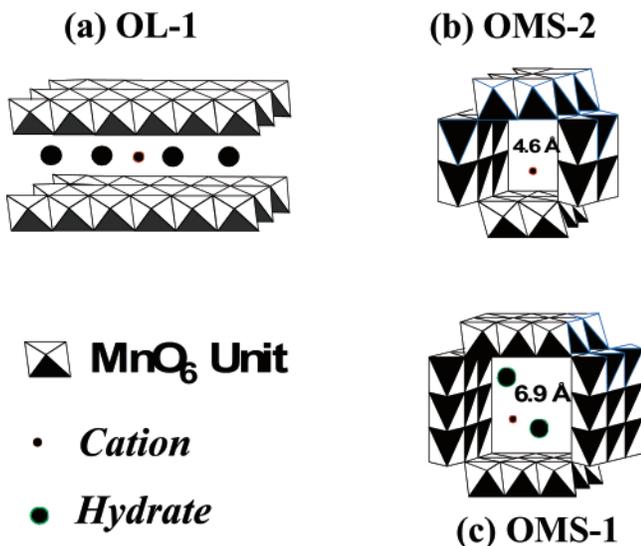- • *Cation*
- • *Hydrate*

(c) OMS-1

Figure 1. Scheme showing structures of layered and tunnel manganese oxides: (a) OL-1; (b) OMS-2; (c) OMS-1.

limitations of nitrogen molecules to access into the narrow pores of this material at liquid-nitrogen temperature (77 K), as previuosly observed for other microporous solids with similar pore diameters, like Zeolite NaA.[21] In this study, we used CO_2 physisorption at 273 K to confirm the microporous nature of this material and the suitability of this technique to characterize the texture of materials with narrow porosity (less than 0.6 nm).

In previous work we synthesized OMS-2 catalysts and evaluated their performance in the total oxidation of benzene, ethanol, and hexane. The extremely high selectivity and activity observed in such studies has suggested that these materials act like enzyme catalysts where substrates fit in a lock and key type mechanism.[33,34] OMS-2 has shown to be most active among several types of manganese oxides. In this work, studies on the physical and chemical adsorptive properties, porosity, acid–base properties, hydrophobic features of OMS-2, and facile evolution of lattice oxygen atoms and recovery are conducted. Reactions, as well as temperature-programmed surface reactions, with or without addition of gaseous oxygen have been used to elucidate the mechanism, especially to distinguish the roles of lattice oxygen and gaseous oxygen in oxidation. A typical commercial catalyst Pt/Al$_2$O$_3$ was used for comparison.

2. Experimental Section

2.1. XRD, HRSEM, and ICP-AES for Characterization of OMS-2 and Other Catalysts. The syntheses of various types of manganese

oxide catalysts and terminologies were reported in previous work.[18,30–32] NaOH–OMS-2 was prepared after OMS-2 was synthesized, washed, and then treated with a solution of NaOH (2 M) for 1 h and then washed and dried. Other post-treatment processes are the same as those of OMS-2.

X-ray diffraction experiments were done on a Scintag XDS 2000 X-ray diffractometer using a tube voltage of 45 kV and a tube current of 40 mA with Cu Kα radiation. XRD patterns were taken in a continuous scan mode at a scanning speed of 5 deg 2θ/min. The instrument was calibrated using α-quartz as an external standard. The sample (fresh or after reaction or other experiments) was ground (particle size <1 μm) and placed into a sample holder for experiments.

2.2. IR and Adsorbate IR and Acidity. The IR experiments were done on a Nicolet Magna-IR System 750 FT-IR spectrometer equipped with an in-situ cell for heating, adsorption, and reactions. To take IR spectra, standard procedures of single beam diffuse reflectance methods with an MCT-B detector and a KBr beamsplitter were employed, with 200 scans collected at a resolution of 4 cm^{-1}. The sample powders were put in a desiccator containing a saturated solution of NH$_4$NO$_3$ for overnight sorption of water.

To detect adsorbed species, a sample was heated in the IR cell at 200 °C for 4 h while purging with air. After the heated sample was cooled to room temperature, a flow of air saturated with adsorbate (ethanol, benzene, and or water) was introduced for adsorption for 10 min. Extra adsorbate was removed with a nitrogen flow before IR spectra were taken. In surface acidity studies, a flow of nitrogen was used to transport pyridine vapor for adsorption (10 min) and a flow of pure nitrogen was used to remove extra vapor (30 min) from the surface area.

2.3. TGA, DSC, TPD-MS, and TPSR-MS. TGA profiles were made on a Hi-Res TGA 2950 thermogravimetric analyzer (TA instruments). DSC experiments were carried out on a DSC 2900 differential scanning calorimeter (TA instruments). The samples were heated in nitrogen or oxygen from room temperature to a required temperature at a rate of 10 °C/min and held at the final temperatures for 10 min.

In TPD-MS (temperature-programmed decomposition–mass spectroscopy) experiments, 0.1 g amounts of samples were placed in a U-type quartz tube which was placed in a temperature-programmable furnace. The sample was purged in He to remove adsorbed air and heated at 10 °C/min in He to 700 °C, with the downstream gas monitored with an MKS–UTI quadrupole mass spectrometer. In temperature-programmed surface reaction (TPSR) experiments, a sample (0.1 g) was heated at 250 °C for 1 h and cooled to room temperature for adsorption of benzene (benzene vapor saturated at 0 °C with He). Helium was then flowed through the sample to remove excess benzene (monitored by MS) before TPSR-MS studies.

2.4. Sorption Experiments. 2.4.1. Nitrogen and CO_2 Adsorption. Nitrogen physisorption experiments were done at 77 K using an ASAP 2100 physisorption apparatus, and CO_2 physisorption experiments were carried out in an Autosorb-6 apparatus at 273 K using an ice-bath. The Dubinin–Radushkevich equation was used to estimate micropore volumes from physisorption data.[22,23] The densities used for the N_2 and CO_2 physisorbed in the various porous solids studied were 0.808 and 1.023 g/cm^3, respectively.[21,24–26]

2.4.2. Chemical Adsorption. Sorption of water, methanol, benzene, or binary mixtures of the above-mentioned adsorbates in static and flow environments was studied at room temperature with static weighing. Samples (ca. 0.20 g, after being pressed, crushed, and sieved to 20–40 mesh) were heated at 250 °C for 4 h and put in a desiccator containing saturated solutions of NH$_4$NO$_3$ of water, ethanol, or benzene for sorption of water, ethanol, or benzene, respectively, and containing

(22) Dubinin, M. M. *Chem. Rev.* **1960**, *60*, 235−241.
(23) Dubinin, M. M. *Chemistry and Physics of Carbon*; Marcel Dekker: New York, 1966; Vol. 2, p 1.
(24) Reinoso, F. R.; Solano, A. L. *Chemistry and Physics of Carbon*; Marcel Dekker: New York, 1994; Vol. 21.
(25) Amorós, D. C.; Momge, J. A.; Solano, A. L. *Langmuir* **1996**, *12*, 2820−2824.
(26) Amorós, D. C.; Momge, J. A.; de la Casa-Lillo, M. A.; Solano, A. L. *Langmuir* **1998**, *14*, 4589−4596.
(27) Ehrburger-Dolle, F.; Holz, M.; Lahaye, J. *Pure Appl. Chem.* **1993**, *65* (10), 2223−2230.
(28) Suib, S. L.; O'Young, C. L. In *Synthesis of Porous Materials*; Occelli, M. L., Kessler, H., Eds.; Marcel Dekker, Inc.: New York, 1997; pp 215−231.
(29) O'Young, C. L.; Sawicki, R. A.; Suib, S. L. *Microporous Mater.* **1997**, *11*, 1−8.
(30) Luo, J.; Zhang, Q.; Huang, A.; Suib, S. L. *Microporous Mesoporous Mater.* **2000**, *35−36*, 209−217.
(31) Luo, J.; Huang, A.; Park, S.; Suib, S. L.; O'Young, C. L. *Chem. Mater.* **1998**, *10*, 1561−1568.
(32) Luo, J.; Tan, C.; Dong, Q. *Fuel Chem. Technol.* **1990**, *18*, 207−216.
(33) Son, Y. C.; Makwana, V. D.; Howell, A. R.; Suib, S. L. *Angew. Chem., Int. Ed.* **2001**, *40*, 4280−4283.
(34) Makwana, V. D.; Son, Y. C.; Howell, A. R.; Suib, S. L. *J. Catal.* **2002**, *210*, 46−52.

water/ethanol or water/benzene mixtures (contained in different beakers) for sorption experiments.

Adsorption of water at various partial pressure of water was done in a flow system. An activated sample in a weighing vial was put in a desiccator at room temperature, with a flow of nitrogen of different moisture level (one flow passes through a moisture saturator and another flow is used to dilute the saturated gas) for 2-h moisture uptake. Accurate weighing was done before and after sorption to obtain the uptake amount.

2.5. Catalytic Evaluation in Continuous and Other Reactions. Catalysts (0.12 g, pressed and sieved to 20−40 mesh) were placed in a U-type stainless steel reactor packed with quartz wool. A thermocouple was attached to the external surface of the reactor at the catalyst bed to record reaction temperatures. After the catalyst was pretreated at 250 °C in flowing air for 1 h, the temperature was lowered to 100 °C and then the reaction was started. Benzene vapor was transported into the reactor by using air as carrier gas flowing through a benzene-containing bubbler placed in an ice bath. Another flow of air was used to dilute the reactant. By adjustment of the two flow rates (controlled by a flow controller), the concentration of benzene in the reactant was regulated to be 0.1%−3.5%. Under our reaction conditions, both internal and external diffusional resistances have been eliminated if reaction temperature was above 200 °C, as confirmed by experiments with different linear velocities and different sizes of catalysts.

From the conversion vs temperature curve for the reaction of 0.9% benzene in air and GHSV 20000 h^{-1}, the temperature corresponding to a 50% conversion is defined as the half conversion temperature, T_{50}. This temperature is used to compare the oxidation efficiency of the catalysts (Figure 10 and Table 3). The lower the temperature T_{50} is, the higher is the oxidation efficiency of the catalyst.

Reactions of CO were done at room temperature using a glass frit reactor. The internal resistance could not be eliminated at this temperature with a size even under 20 mesh. The powder form of the catalyst was used. After reaction the reactor was washed with concentrated HCl to dissolve any manganese oxide catalysts left in the frit. A reactant of 1.0% CO in He was used for mixing with a pure helium and/or oxygen to make different reactants.

Analyses of reaction products were done on-line either with a Q-MS or an HP 5990 A GC gas chromatograph (GC) equipped with a thermal conductivity detector (TCD), an HP 3395 integrator, and a 30 m × 0.32 mm × 0.25 μm HP-5 capillary column. The downstream gas was connected to another HP 5990 A GC with a TCD and a 25-foot Carboxen 1000 packed column for analyses of O_2, N_2, CO, and CO_2. Helium was used as a carrier gas for all analyses. Concentrations are determined by external standard methods for calculations of conversions. Relative errors of these GC analyses are within 5%. At each temperature or flow rate, analyses of reaction products were taken at a time-on-stream of 30 min unless otherwise mentioned.

3. Results

3.1. Structure, Morphology, and Composition of Catalysts. OMS-2 is a black solid, consisting of uniform fibers of ca. 0.1 × 1 μm, as shown by scanning electronic microscopy (Figure 2). XRD pattern shows a typical cryptomelane structure (Figure 3). This structure is stable after all the reactions and treatments, except for TGA-DSC studies or for calcination over 650 °C. The compositional data for prepared OMS-2 and NaOH solution treated OMS-2, as well as OL-1, OMS-1, and other catalysts as obtained from ICP-AES analyses and oxalate titration methods (water contents were determined by weight loss in static heating at 180 °C for 2 h),[30] are listed in Table 1.

3.2. IR Studies for Surface Species and Acidic Properties. Figure 4 shows IR spectra of the samples. IR peaks at 600 and 520 cm^{-1} are characteristic of cryptomelane.[7] No IR bands were
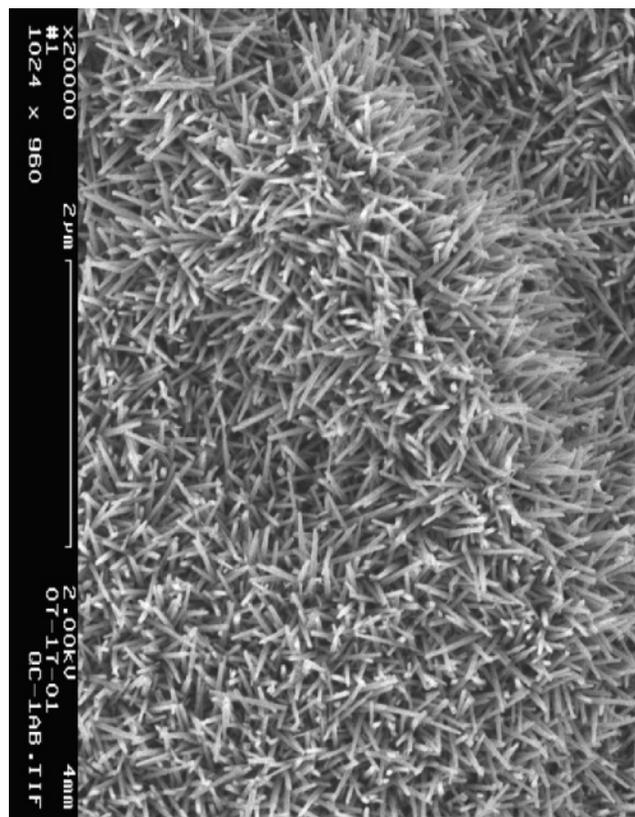
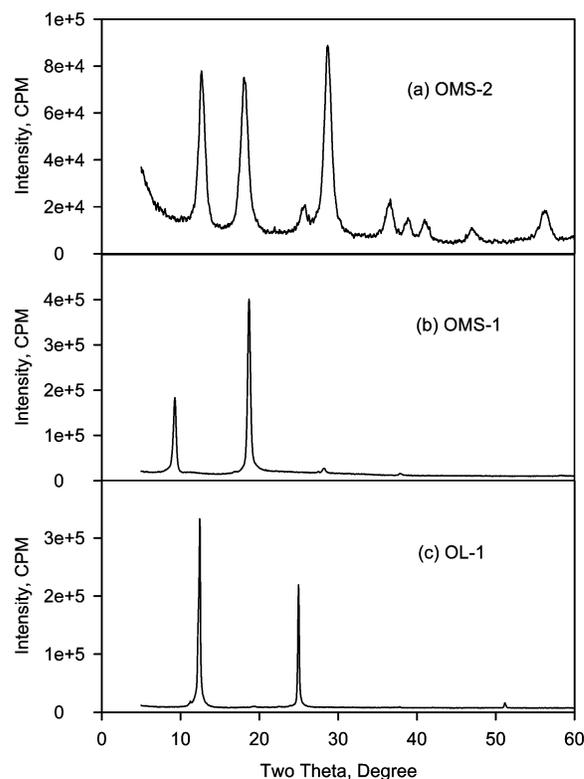**Figure 2.** SEM photographs of OMS-2.

Figure 3. XRD patterns of OL-1, OMS-1, and OMS-2.

observed in the region 3000−3700 cm^{-1}, showing no hydrates or sorbed water in the OMS-2 product. On the contrary, OL-1, OMS-1, and Na−ZSM-5 (a high-silica pentasil zeolite molecular sieve with ca. 6 Å openings[16,17,33]) all showed very strong IR

Table 1. Composition and Surface Area[a] of Catalysts Used in This Study

catal	composn	$S_{BET}(N_2)$ $(m^2/g)^a$	$S_{micro}(CO_2)$ $(m^2/g)^b$
OL-1	$Na_{0.39} \cdot Mg_{0.042} \cdot 0.044MgO \cdot MnO_2 \cdot 0.77H_2O$	57	205
OMS-1	$Na_{0.014} \cdot Mg_{0.24} \cdot 0.051MgO \cdot MnO_2 \cdot 0.92H_2O$	71	256
OMS-2	$K_{0.07}H_{0.08} \cdot MnO_2 \cdot 0.085H_2O$	97	272
NaOH− OMS-2	$K_{0.07}Na_{0.08} \cdot MnO_2 \cdot 0.082H_2O$	95	N/A
Pt/Al_2O_3	1.0% Pt/Al_2O_3	160	N/A

[a] As determined by N_2 sorption, total BET surface area, almost no micropore surface area. [b] As determined by CO_2 adsorption, only micropore surface area.
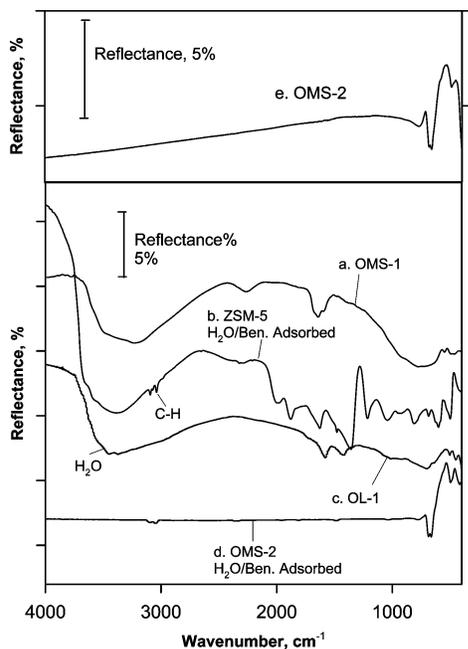
Figure 4. Diffuse reflectance IR spectra of (a) OMS-1 (dried in air), (b) ZSM-5 (a pentasil high-silica zeolite, which is hydrophobic) after adsorption of both benzene and water, (c) OL-1, (d) OMS-2 which has been exposed to water/benzene for sorption, and (e) OMS-2.

absorption in the region $3000-3700$ cm^{-1}, indicative of associated water molecules and/or hydroxyl groups.

A benzene-sorbed OMS-2, however, shows characteristic IR absorption of C−H bands around 3100 cm^{-1}. OMS-2 exposed to both benzene and water shows no absorption of water but only benzene (Figure 4d), indicating that OMS-2 can selectively adsorb organic species. In the static adsorption, OL-1, OMS-1, and ZSM-5 adsorb both water and benzene. These results suggest that the OMS-2 product is hydrophobic.

Pyridine adsorbate IR data are shown in Figure 5. The bands at 1550 cm^{-1} correspond to Brönsted (B) acid sites while those at 1450 cm^{-1} are aroused from Lewis acid (L) sites, representing protonated and coordinated pyridine, respectively.[20] A sample of OMS-2 treated with solutions of NaOH (2 M) showed only Lewis acid sites. The B acid sites disappear after base treatment. Under similar conditions, L acid sites (IR band at 1450 cm^{-1}) were also observed with OL-1, with no B acid sites detected. For OMS-1, both B and L acid sites were detected, with the intensity of B acid sites slightly lower than that with OMS-2.

3.3. Adsorption and Pore Structure. Nitrogen isotherms at 77 K of OMS-1 and OMS-2 materials, their surface areas, and micropore volumes, are shown in Figure 6 and Tables 1 and 2,
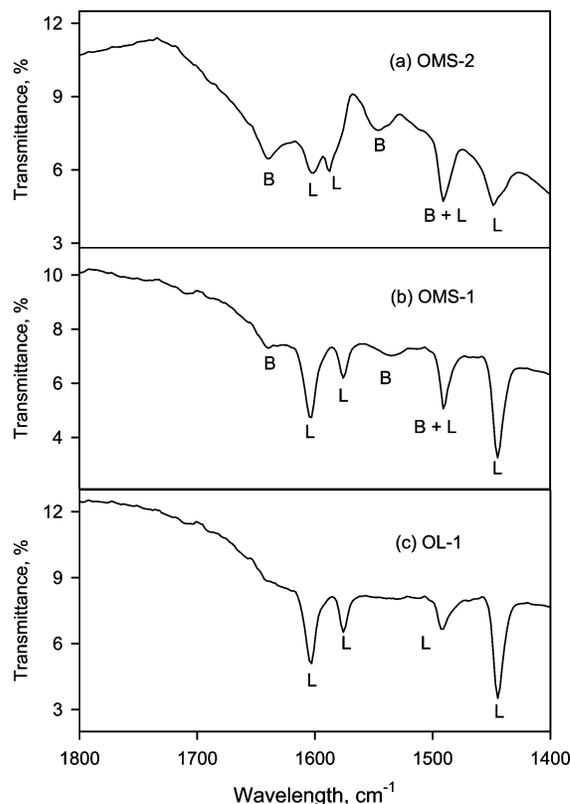
Figure 5. Pyridine adsorbate IR spectra (where B acid sites mean Brönsted acid sites and L acid sites mean Lewis acid sites) of (a) OMS-2, (b) OMS-1, and (c) OL-1.
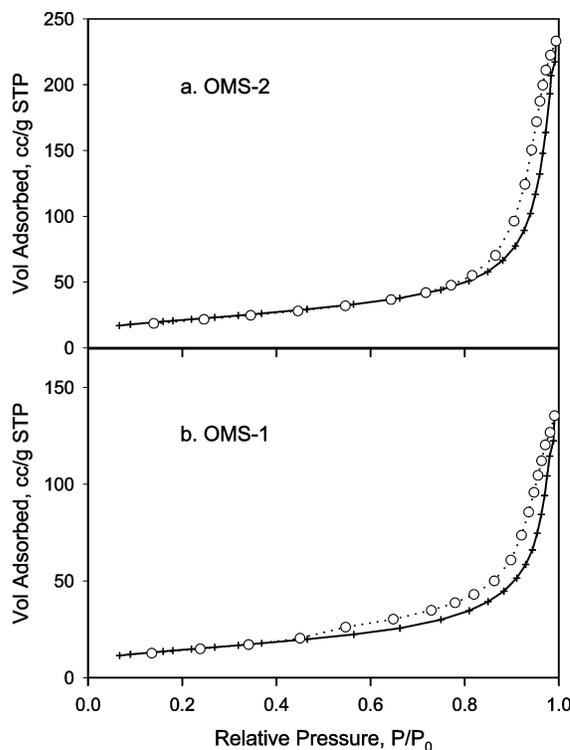
Figure 6. Nitrogen adsorption isotherms (+, adsorption; ○, desorption) of OMS-2 and OMS-1.

respectively. From these experiments, OMS-2 (as well as OMS-1) appears to be nonporous, with a negligible micropore volume (0.002 cm^3/ g; see Table 2). For comparison purposes, zeolite ZSM-5 has been quoted in this study, showing a typical type I

Table 2. Uptake (wt %) of Water, Ethanol, Benzene, and Water/Benzene and Pore Volumes (cm³/g) Based on CO_2 and N_2 Physisorption at 273 and 77 K, Respectively, Using the Dubinin−Radushkevich Method of Cryptomelane-Type Octahedral Molecular Sieves and Other Materials Used for Comparative Purposes

	uptake of adsorbates (wt %)						
adsorbents[a]	water	ethanol	benzene	water/benzene	H-index	CO_2 V_{DR} (cm³/g)	N_2 V_{DR} (cm³/g)
Na−ZSM-5	9.1	9.8	12.4	10.3	0.32	N/A	0.16
OL-1	17.3	9.5	3.0	13.9	0.05	0.08	0.0005
OMS-2	2.0	7.7	9.1	7.9	1.05	0.10	0.0019
NaOH−OMS-2	1.8	N/A	N/A	N/A	N/A	N/A	0.0018
OMS-1	13.7	8.7	9.6	7.5	0.15	0.10	0.0021

[a] Static sorption experiments were done at 27 °C in a desiccator containing a saturated solution of NH_4NO_3 of each of the adsorbates (with different polarity) used in this study.
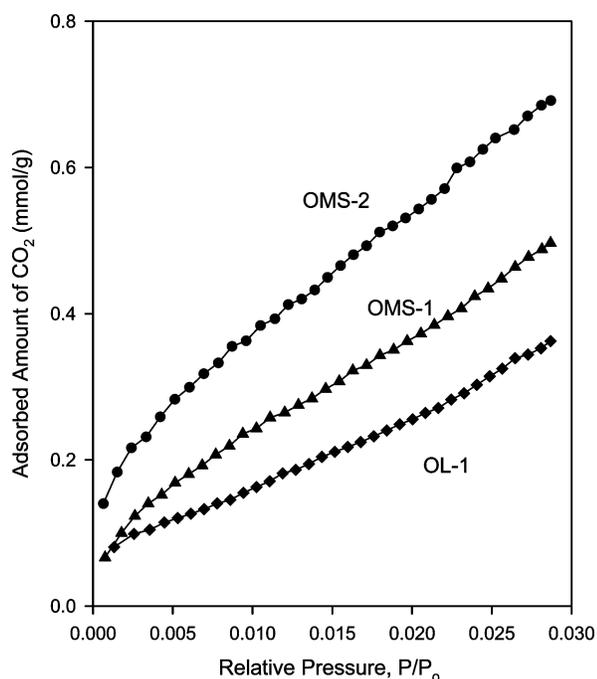

Figure 7. CO_2 physisorption isotherms at 273 K of OMS-1, OMS-2, and OL-1 materials.

Figure 8. Water adsorption isotherms of OMS-2 and others.

isotherm,[32] characteristic of microporous materials. Figure 7 presents the CO_2 isotherms at 273 and subatmospheric pressure of OMS-1, OMS-2, and OL-1 materials. These experiments show that CO_2 at 273 K can indeed access the narrow microporosity of OMS-2 at 273 K, giving a notable micropore surface area (250−270 m²/g) and micropore volume (~0.1 cm³/g), corresponding to its crystalline microporous structure (see Table 2).

A water adsorption isotherm is shown in Figure 8. OMS-2 showed by far the lowest overall water uptake among the catalysts used at all the relative moisture levels, even at saturated pressure. Although these materials are all porous, their adsorptive properties are quite different. At low humidity, very low water uptake was obtained with OMS-2 and relatively small water uptake with ZSM-5. Both OL-1 and OMS-1 showed very high uptake of water even at low relative humidity. This indicates the formation of interlayer and tunnel hydrates among OL-1, OMS-1, and, to a smaller extent, ZSM-5. Throughout the humidity range OMS-2 showed little water uptake.

Static adsorption results are listed in Table 2. OMS-2 shows the smallest uptake of water, a large part of which can easily be removed by purging with a flow of dry gas. OMS-2 exhibited relatively large uptakes of ethanol and benzene, showing a stronger affinity for organic species. In addition, sorption
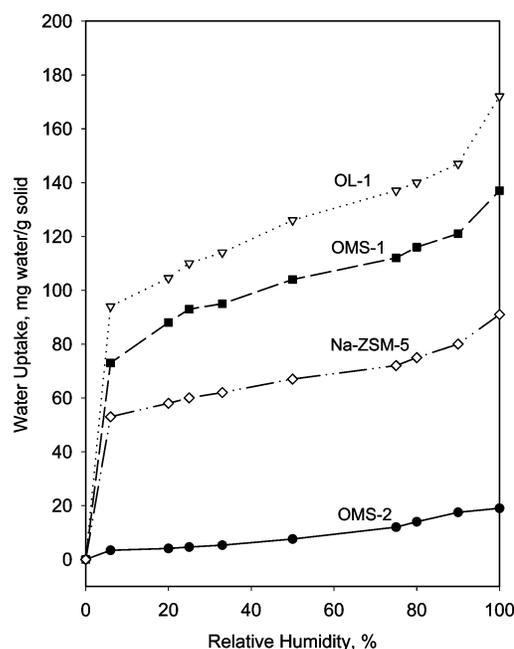
experiments with mixtures show that OMS-2 adsorbs large amounts of water/benzene and water/ethanol in air. However, adsorbate IR studies only show organic species on samples of OMS-2 exposed to water/benzene or water/ethanol. This indicates that OMS-2 selectivity adsorbs organic species in the presence of water.

3.4. Thermal Stability, Lattice Oxygen Evolution, and Recovery. OMS-2 showed only small weight losses before 150 °C due to the loss of water in TGA studies (Figure 9a) and no DSC endothermic peaks before 150 °C accounting for water evaporation (in air), as compared with weight losses of ca. 12−20 wt % and large endothermic peaks with OL-1 and OMS-1.[18] Weight losses at higher temperatures (>200 °C) are due to the evolution of oxygen from the lattice, as confirmed by temperature-programmed decomposition in helium with mass spectroscopic detection. OMS-2 decomposes to bixbyite, Mn_2O_3, in air upon heating over 650 °C and to hausmannite, Mn_3O_4, over 800 °C, as confirmed by XRD. In a nitrogen flow, the evolution of oxygen occurs at much lower temperatures as compared to that in oxygen or air stream, starting at 130 °C while the decomposition of OMS-2 starts at 520 °C. XRD data show that OMS-2 is stable below 650 °C in air and below 500 °C in nitrogen or helium under static heating. OMS-2 is far more thermally stable than OL-1 and OMS-1, whose decomposition temperatures are below 400 °C under in air.[18]
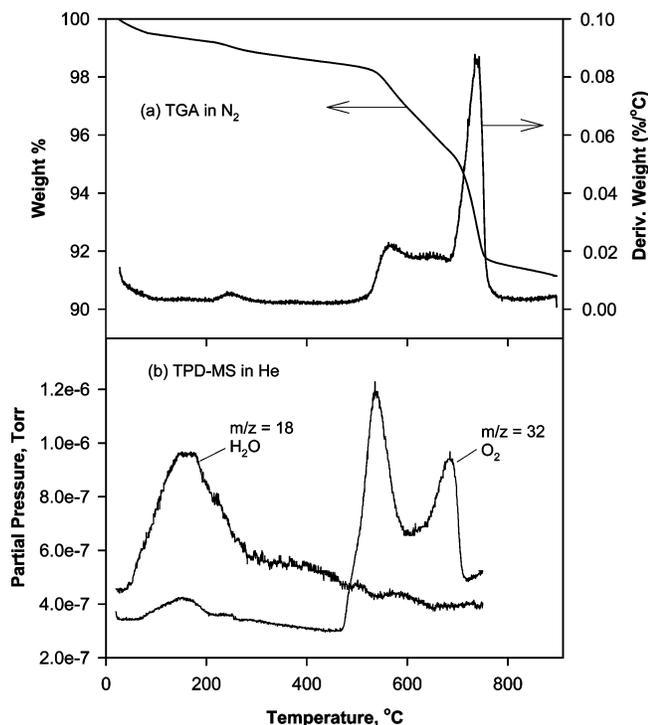
Figure 9. TGA and TPD-MS profiles of OMS-2 showing reversible oxygen evolution.

Figure 10. Total oxidation of benzene (reactants are 0.9% benzene in air, GHSV 20000 h^{-1}) on layered and tunnel manganese oxides and Pt/Al$_2$O$_3$.

TPD-MS data for a fresh OMS-2 sample (heated at 10 °C/min in He, with the downstream gas monitored with a mass spectrometer) show similar results. Small desorption of water was observed below 200 °C, with a release of oxygen starting at ca. 100 °C and continuing above 800 °C. XRD results show that OMS-2 is stable even above 650 °C under static heating. These experiments suggest that oxygen species are released from the OMS-2 lattice without destroying the crystal structure, forming oxygen vacancies which may be catalytically active sites. Neither ZSM-5 nor Pt/Al$_2$O$_3$ exhibits any oxygen evolution, except loss of water upon heating under the same conditions.

When the TGA of OMS-2 in air is stopped at 650 °C for 10 min and then cooled in air, oxygen uptake by OMS-2 is observed by a weight gain of 0.47 wt % from 650 to 30 °C and 0.09 wt % from 180 to 30 °C. (The weight gain was not observed in TGA with N$_2$.) In DSC, the heating/cooling of OMS-2 in air below 650 °C does not show any peaks indicating no phase change in this temperature range. This oxygen uptake is not observed with ZSM-5 nor with Pt/Al$_2$O$_3$. No significant difference in TGA-DSC was observed with the NaOH-treated OMS-2 sample. For OMS-1 and OL-1, similar oxygen evolution and reversible recovery can be observed within a much lower temperature range, below 400 °C, higher than which the samples are converted into a hausmannite structure, Mn$_3$O$_4$.[18]

3.5. Total Oxidation of Benzene with OMS-2. Total oxidation of benzene was tested at 100−400 °C, 0.1%−3.5% benzene/air, and flow rate of 15−180 mL/min. Under these conditions the activities are stable for all three catalysts tested, even at the upper temperature limits of the reactions. The dependence of conversion of benzene on temperature for the oxidation of 0.9% benzene in air and GHSV 20000 h^{-1} over various catalysts is shown in Figure 10. On OMS-2, the oxidation of benzene started at 100 °C with a conversion of
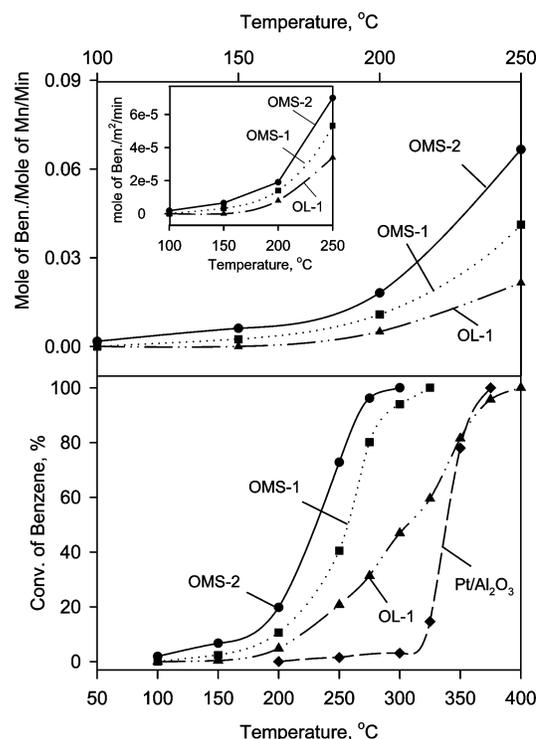
1.9%. As reaction temperature was increased, the conversion increased sharply, reaching 100% below 300 °C, achieving the total oxidation of benzene, with only products of CO$_2$/H$_2$O being observed.

OL-1, OMS-1, Pt/Al$_2$O$_3$, and NaOH−OMS-2 were also tested under identical conditions. For catalysts OL-1 and OMS-1, oxidation of benzene started at significantly higher temperatures (150 and 200 °C, respectively) as compared with that over OMS-2 (100 °C). No activity was observed at 100 °C for OMS-1 and at 150 °C for OL-1. Although trends similar to those of OMS-2 with respect to temperature dependence were observed, both catalysts showed much lower activity than OMS-2, especially at lower temperatures (Figure 10a). These results indicate that OL-1 and OMS-1 are much less active in total oxidation of benzene than OMS-2. Detailed comparisons in terms of activity/active sites (turnover number) or activity/surface area are given in Figure 10b. OMS-2 is obviously more active than OMS-1 and OL-1.

When the catalyst OMS-2 is treated with NaOH solutions, dried, and activated in the same manner as with regular OMS-2 samples and tested in reaction, the activity in benzene oxidation decreases substantially at all temperatures, with activities between OMS-2 and OMS-1 at all temperatures. The oxidation of benzene over Pt/Al$_2$O$_3$ starts at a much higher temperature as compared to all manganese oxide catalysts, showing virtually no activity below 300 °C. However, the activity increased sharply over 300 °C, reaching 100% conversion at 400 °C. The half conversion temperatures (T_{50}) for OMS-2, NaOH−OMS-2, OMS-1, OL-1, and Pt/Al$_2$O$_3$ are estimated from Figure 10 to be 230, 245, 255, 310, and 340 °C, respectively (Table 3). This indicates a sequence of decreasing oxidation efficiency under these experimental conditions.

The catalytic performance of OMS-2 in the oxidation of other organic compounds was also tested. Under similar conditions,

Table 3. Surface Acidity of Catalysts Used in This Study, Reversible Lattice Oxygen Dislodgement and Recovery, and Half-Oxidation Temperature

catal	B-acid, IR intensity[a]	L-acid, IR intensity[b]	O-reversibility[c]	T_{50} (°C)
OL-1	no	strong	yes	310
OMS-1	medium	strong	yes	255
OMS-2	strong	strong	yes	230
NaOH−OMS-2	no	strong	yes	245
Pt/Al$_2$O$_3$	no	strong	no	340

[a] The intensity of IR bands around 1540 cm^{-1}. [b] The intensity of IR bands around 1450 cm^{-1}. [c] Lattice oxygen reversibly dislodging/recovery during TPD−MS experiments.
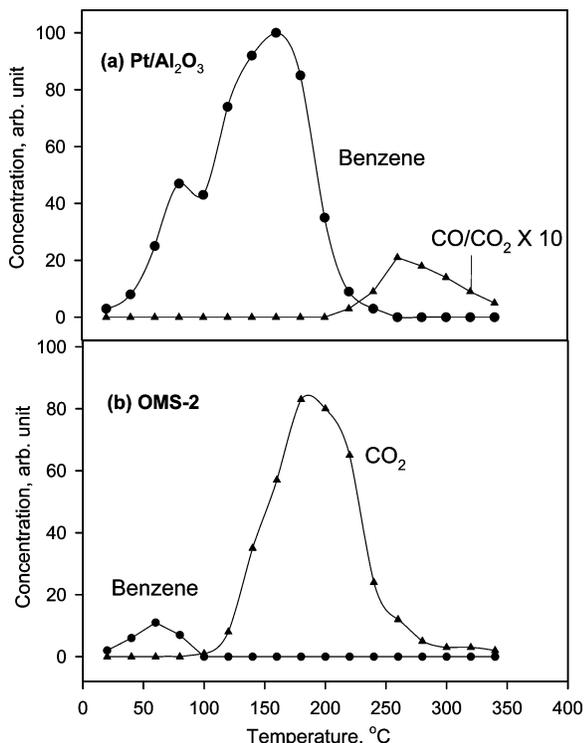
Figure 11. Temperature-programmed surface reaction of benzene on OMS-2 and Pt/Al$_2$O$_3$.

the total oxidation of ethanol can be achieved in a similar manner over OMS-2 at lower temperatures (ca. 200 °C) while propane oxidation needs a higher temperature (ca. 375 °C) to achieve 100% conversion.

3.6. Temperature-Programmed Reaction and Reactivity of Lattice Oxygen. 3.6.1. Lattice Oxygen Reaction with Benzene. A benzene-adsorbed OMS-2 was tested for temperature-programmed surface reaction (TPSR) in a flow of helium (Figure 11). As temperature increases over 100 °C, adsorbed benzene began to convert to CO$_2$/H$_2$O. The process ends before 300 °C. No desorption of benzene or formation of CO was observed in this experiment, even at lower temperatures. Unlike the case of only temperature ramping with TPD-MS (where oxygen evolution was observed), no oxygen evolution was observed in the TPSR-MS. The only products are H$_2$O and CO$_2$ which should be formed from oxidation of absorbed benzene. Under the same conditions, only desorption of benzene was observed for a benzene-adsorbed ZSM-5 or Pt/Al$_2$O$_3$ in this study, showing no oxidation even at the end of desorption (<250 °C). This study shows that the lattice oxygen of OMS-2 can react with adsorbed benzene species. ZSM-5 and Pt/Al$_2$O$_3$ will
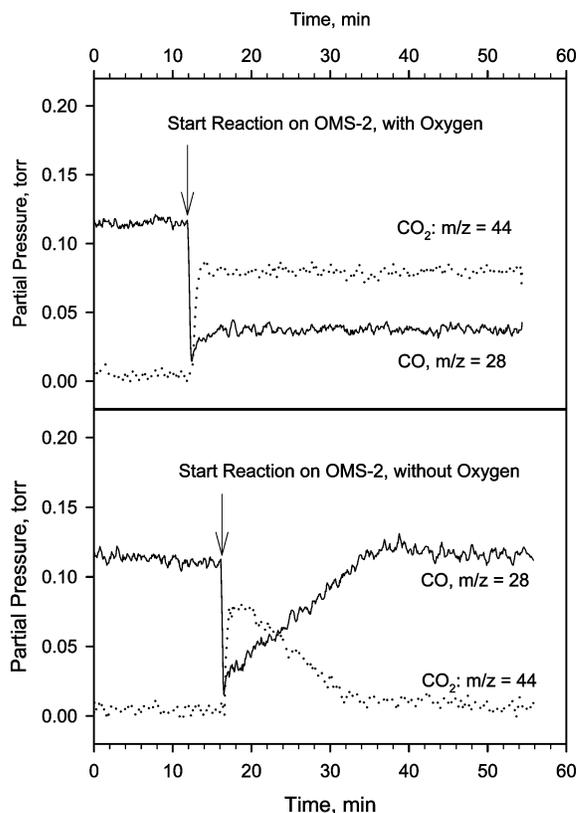
Figure 12. Reaction of benzene on OMS-2 (200 °C, b) and Pt/Al$_2$O$_3$ (300 °C, a) with (solid lines) and without (dotted lines) gaseous oxygen.

not react with benzene even at elevated temperature if external gaseous oxygen is not present.

The TPSR results are to test the effects of lattice oxygen on reaction. TPSR does not distinguish the function of gaseous oxygen in the presence of catalyst. To study the effects of both gaseous and lattice oxygen, the following tests were conducted (Figure 12). The oxidations of 0.1% benzene + 20% O$_2$ in He and 0.1% benzene in He (no oxygen) were conducted over OMS-2 (GHSV 10000 h^{-1}, 200 °C) and over Pt/Al$_2$O$_3$ (GHSV 10000 h^{-1}, at 300 °C) for comparison. The downstream gases were monitored with a Q-MS.

For OMS-2, a stable conversion of 30−34% as determined by the Q-MS signal intensities is obtained in the case of the oxygen containing reaction. The initial conversion is similar when oxygen is absent. However, the initial activity can only last about 3 min, gradually decreasing to zero in about 20 min. From the concentration of benzene, conversion, and time of reaction, it is estimated that about lattice oxygen of 1.0% of the weight of cryptomelane catalyst (or ca. 3% of total lattice oxygen for a MnO$_2$) was consumed in the oxygen-free oxidation of benzene. When the deactivated catalyst is purged with air and the reaction is resumed, the activity can almost be totally recovered. Similar results can be obtained with other manganese oxide catalysts. No reaction can be observed with Pt/Al$_2$O$_3$ at this temperature. A higher temperature (300 °C) is needed for reaction to occur. At 300 °C, the conversion is stable on Pt/Al$_2$O$_3$ and over 50% when oxygen is present. However, almost no oxidation is observed when oxygen is absent.

3.6.2. Reaction of Gaseous and Lattice Oxygen with CO. The results for CO oxidation with 0.1% CO + 20% O$_2$ in helium over OMS-2, base-treated OMS-2, and Pt/Al$_2$O$_3$ are shown in
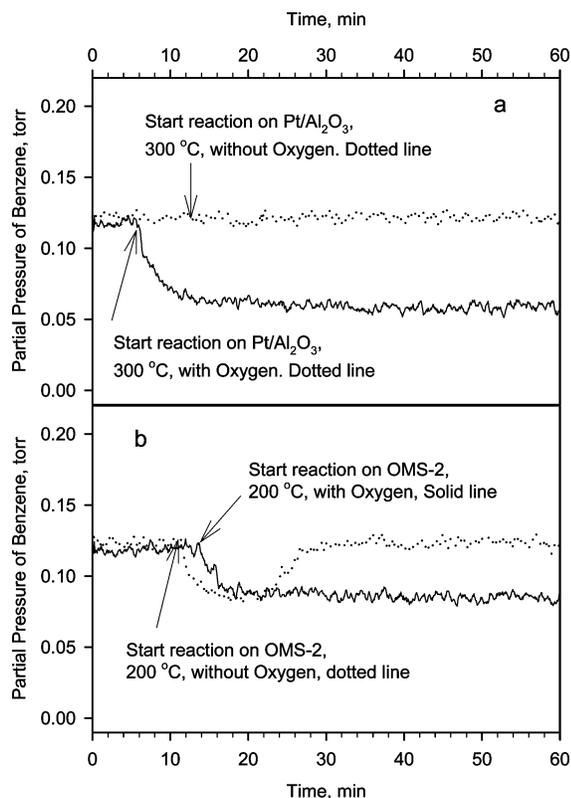
Figure 13. Room-temperature CO oxidation on OMS-2 with and without gaseous oxygen, as monitored with Q-MS signals of CO (solid lines, m/z 28) and CO_2 (dotted lines, m/z 44).

Figure 14. Room-temperature CO Oxidation on Pt/Al_2O_3 with and without gaseous oxygen, as monitored with Q-MS signals of CO (solid lines, m/z 28) and CO_2 (dotted lines, m/z 44).

Figures 13 and 14 (GHSV 35000 h^{-1}, room temperature). All three catalysts are very active. The activity is in the order of OMS-2 (conversion ~65%) ~ Pt/Al_2O_3 (~58%) > NaOH−OMS-2 (~40%).

The reaction with reactant 0.1% CO in helium (no oxygen) is conducted to study the function of lattice oxygen. Without external gaseous oxygen, Pt/Al_2O_3 does not show any activity. OMS-2, however, shows the same initial activity as that with oxygen. However, the activity decreases rapidly all the way to zero in about 12 min. When air is used to purge the deactivated catalysts (10 min, which is then purged with He), the activity with the oxygen-free reactant (0.1% CO in He) can be recovered. But again, the initial activity will be lost in ca. 12 min. From the concentration of CO, conversion, and reaction time, lattice oxygen of ca. 0.35% in weight of the cryptomelane catalyst (or ca. 1% of total lattice oxygen of cryptomelane) was consumed in the reaction. XRD data show that the catalyst still retains the structure of cryptomelane after the reaction.

4. Discussion

IR and adsorption experiments show that OMS-2 prepared in this study is porous, acidic, and hydrophobic. The large porosity and surface area suggest excellent accessibility of active sites to reactant molecules. Acidity relates to the interaction between the catalyst and any basic molecules (B and L). The hydrophobicity suggests a smaller adsorption of moisture on the surface, which should lead to better durability for reactions in the presence of moisture. Other catalysts are different in their acidic properties (Table 3). TPD-MS, TGA/DSC, and static heating experiments show that OMS-2 studied here is thermally stable in air (>650 °C). However, some of the oxygen in the
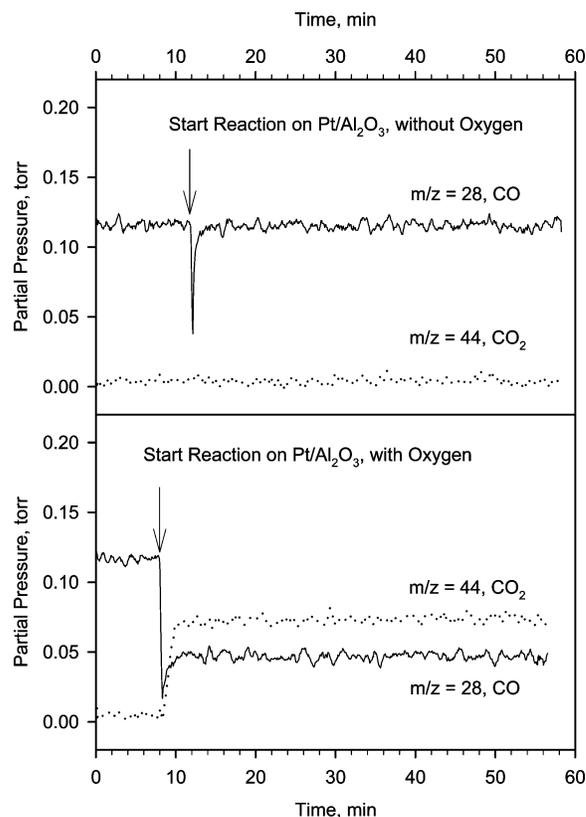
OMS-2 framework can easily dislodge from the framework without destroying the overall framework structure when the sample is heated in air at as high as 650 °C, as shown herein and in previous work.[30,35,36,38] The desorption of lattice oxygen is reversible. Other MnO_x-based catalysts are also like this but have different thermal stabilities. These results are listed in Tables 1−3 and are all common properties relevant to the oxidation reaction.

Noticing that the compositions are slightly different (the major part is MnO_x with Mg in OL and OMS-1 for structure-templating agents[19]) for the manganese oxides (Table 1), we prepared Mg-free and Na-free OL-1 (using KOH to replace NaOH in the synthesis) and tried to adjust the starting MnO_4^-/Mn^{2+} ratios[18] to make the composition ($K_{0.19} \cdot MnO_2 \cdot 0.8H_2O$) of OL-1 very close to that of OMS-2 and then tested the activity in benzene oxidation. Under similar conditions, the activity of Mg-free OL-1 showed only slightly higher conversion than that of regular OL-1, with a relative difference within 5%. These data therefore indicate that these differences in activity are not primarily due to slight differences in composition of the MnO_x but are due to differences in other properties. The effects of important properties related to catalytic functions are discussed below.

(35) Yin, Y. G.; Xu, W. Q.; DeGuzman, R.; Suib, S. L.; O'Young, C. L. *Inorg. Chem.* **1994**, *33*, 4384−4389.
(36) Yin, Y. G.; Xu, W. Q.; Shen, Y. F.; Suib, S. L.; O'Young, C. L. *Chem. Mater.* **1994**, *6*, 1803−1808.
(37) Rouquerol, L.; Avnir, D.; Fairbridge, C. W.; Everett, D. H.; Haynes, J. H.; Pernicone, N.; Ramsay, J. D. F.; Sing, K. S. W.; Unger, K. K. *Pure Appl. Chem.* **1994**, *66*, 1739−1758.
(38) Zhang, Q.; Luo, J.; Vileno, E.; Suib, S. L. *Chem. Mater.* **1997**, *9*, 2090−2095.

4.1. Physical Adsorption and Microporisity. From a structural viewpoint, the micropore porosity of OMS-1 and OMS-2 can be estimated by assuming that the tunnels are composed of MnO_2 units. The structural building blocks should be MnO_6 units, with each oxygen atom shared by three octahedral units, and therefore, the simplest structural formula is MnO_2, with each structural unit being shared by two tunnels. For example, four octahedra of OMS-2 (eight octahedra, each shared by two tunnels) form a tunnel space of approximately 4.7×4.7 Å (1 Å $= 10^{-8}$ cm $= 10^{-10}$ m) and 2.3 Å, and therefore, the tunnel porosity and tunnel surface free of any in-tunnel species should be estimated as expressed in the following:

$$(6.02 \times 10^{23} \text{ mol}^{-1}) \times (4.7 \times 10^{-8} \text{ cm})^2 \times$$
$$(2.3 \times 10^{-8} \text{ cm})/(4 \times 87.5 \text{ g/mol}) = 0.09 \text{ cm}^3/\text{g} \quad (1)$$

$$(6.02 \times 10^{23} \text{ mol}^{-1}) \times (4 \times 4.7 \times 10^{-10} \text{ m} \times$$
$$2.3 \times 10^{-10} \text{ m})/(4 \times 87.5 \text{ g/mol}) = 740 \text{ m}^2/\text{g} \quad (2)$$

Similarly, the tunnel porosity and surface area of OMS-1 should be around 0.13 and 740 m²/g, respectively. The microporosity is close to the tunnel volume as obtained from CO_2 adsorption, being 0.1 cm³/g for both OMS-2 and OMS-1. Possibly because more cations such as Mg^{2+}, Na^+, and K^+ are present in the tunnels of OMS-1, the experimental micropore porosity is substantially smaller than the theoretical tunnel porosity. The microporosity of 0.1 cm³/g of the tunnel materials is similar to that of 0.16 cm³/g for zeolite ZSM-5 if a "molar microporosity" is employed, using a simplified chemical formulas of MnO_2 for the tunnel materials and SiO_2 for ZSM-5, obtaining almost equal molar microporosity of 8.8 cm³/mol for OMS-2 and 9.0 cm³/mol for ZSM-5. Due to the two-dimensional structure of OL-1, it is difficult to estimate the microporosity.

The micropore surface areas of both OMS-1 and OMS-2 are only about 1/3−1/2 of the theoretical tunnel surface area, partially due to tunnel ions substantially decreasing the adsorption. As a comparison, almost no micropore volume and micropore surface area can be obtained from nitrogen adsorption experiments. It is noteworthy that people now generally accept that the methods of obtaining micropore surface area might be incorrect (see IUPAC's recommendation[37]). It is therefore less meaningful to compare the micropore surface area.

The limitations of N_2 physisorption at its boiling temperature (77 K) to characterize solids with narrow microporosity (less than 6 Å) like activated carbons, silicas, and zeolites is well-known.[21,24−27] Although, CO_2, and N_2 are rather small molecules (2.8 Å for CO_2 and 3.0 Å for N_2), if the entry of the micropores is too narrow, N_2 at 77 K, due to its low thermal energy and substantial quadrupole moment, suffers from diffusional limitations to access the narrow microporosity (in the case of OMS-2 and OMS-1, the cations in the tunnel should further narrow the space available, especially for OMS-1 with higher ion density in the tunnels) within a reasonable experimental time period. CO_2 at 273, on the contrary, has an activated diffusion, allowing for an accurate determination of microporosity of narrow pores. Therefore this method has been proposed for other authors to characterize materials with narrow microporosity.[21,24]

Similar results, i.e., that N_2 adsorption at 77 K gives unrealistically small pore volumes for other molecular sieves

with similar pore mouth diameters, namely Zeolite NaA (pore mouth diameter 4.1 Å), whereas CO_2 adsorption at 273 provides pore volumes expected from crystallographic data that have been observed previously.[21]

The micropore volumes shown in Table 2 were obtained using the Dubinin−Radushkevich equation:[22,23]

$$V/V_0 = \exp(-1/(E_0\beta)^2 \, (RT \ln(P_0/P))^2) \quad (3)$$

Here V is the volume adsorbed, V_0 the micropore volume, E_0 the characteristic energy dependent on the pore structure, and β the affinity coefficient which is characteristic of the adsorber.

The values obtained from CO_2 at 273 K for OMS-1 and OMS-2 (0.10 cm³/g in both cases, Table 2) are expected for their microporous crystalline structures. However, the porous nature of OMS-2 could not be identified using more conventional N_2 physisorption at 77 K, as repeatedly observed for this material in the past.[28−30] This is the first time that tunnel porosity of OMS-1 and OMS-2 with CO_2 physical adsorption experiments has been demonstrated. Large amounts of micropores that are accessible to reactant molecules at elevated temperature very likely account for the excellent activity of tunnel manganese oxides in selective oxidation reactions.[34,35]

4.2. Hydrophobicity. With static absorption data, a parameter of hydrophobicity index is calculated as the molar ratio of uptake of benzene to uptake of water and listed in Table 2. The larger the index is, the lower the affinity of the material to polar molecules like water. OMS-2 shows the highest hydrophobicity index (1.05) among the materials tested here. Obviously, OMS-2 is highly hydrophobic, even more pronounced than zeolite ZSM-5, a well-known hydrophobic molecular sieve whose hydrophobicity index is determined here to be only 0.32. The much lower values of OMS-1 and OL-1 indicate a high affinity for water. This is consistent with the results of water adsorption in flow systems. Both OMS-1 and OL-1 showed high water uptake even at low humidity, showing that water reacts with OMS-1 and OL-1 forming tunnel or interlayer hydrates, as shown in their structural features.

Adsorption properties are important in catalysis and are usually related to parameters such as porosity, pore size distribution, and intrapore polarity. The special tunnel structure of cryptomelane, together with the relatively high oxidation states of Mn and therefore less intrapore charge density (less polar and therefore smaller affinity for polar molecules of water), may account for the excellent hydrophobicity and strong affinity toward organic compounds. Since water is formed in the oxidation of organic species, the hydrophobic MnO_2 and OMS-2 should therefore show higher activity in total oxidation of organic species to water and CO_2 by favoring the adsorption of organic species and readily repelling water molecules produced from active sites.

4.3. Nature and Functions of Surface Acid Sites. Surface acid sites (B and/or L) are found with many oxides such as alumina and silica and zeolites. B acid sites originate from acidic hydroxyl groups attached to metal atoms, such as Al−OH. L acid sites are regarded as empty orbitals of metal ions in the oxides. In manganese oxides there could be protons from Mn−OH that are acidic and the Mn(IV, III) could have empty orbitals that act as L acid sites.

After base treatment, OMS-2 loses the B acid sites, possibly due to the reaction of protons with hydroxide. The hydroxide

treatment does not affect the empty orbitals of Mn(IV, III), and therefore, NaOH will not affect the L acid sites. The NaOH treatment does not substantially influence the hydrophobicity and lattice oxygen evolution and recovery. NaOH treatment also does not influence the structure. Such base treatment should therefore not affect the micropore structure. In CO oxidation reactions, NaOH−OMS-2 is less active than the original OMS-2 material. These data show that surface acidity plays an important role in the reaction. Surface acid sites might generate preferred adsorption of benzene, CO, and/or oxygen (which are all electron donors) which facilitate oxidation reactions.

In previous work, IR data showed there are hydrates and/or hydroxyl groups in OL and OMS-1 but such species are barely observable with OMS-2.[18,31] However, the density of B acid sites is the highest with OMS-2. At this time it is not clear why no hydroxyl groups are observable with OMS-2 in IR studies. Further study of the nature and functions of surface acid sites with other techniques such as MASNMR (magic angle spin nuclear magnetic resonance) of protons on manganese oxides are under way.

4.4. Reducibility and Reversible Lattice Oxygen Evolution. Manganese oxides are nonstoichiometric oxides with the average oxidative state of Mn changing almost continuously. The evolution of oxygen results in reduced average oxidative state of Mn and the formation of framework oxygen vacancies, which may be catalytically active sites for oxidation reactions. Oxygen species desorbed from the lattice can act as oxidizing agents for CO and VOC's. This might account for the activity of VOC oxidation at relatively low temperatures. Like other MnO_x materials, which are nonstoichiometric oxides with mixed metal valence, OMS-2 can easily react with both reductive and oxidative species without destroying the structure, therefore showing good structural stability under these reaction conditions. This has been investigated in detail in previous work.[38] In return, the good stability of OMS-2 and the facile reversibility of oxygen readsorption may account for the good durability of OMS-2 in oxidation reactions.

The reversible oxygen evolution and reducibility of OMS-2 account for the good performance in oxidation reactions.[34,35] Catalysts without this feature might not be equally active in oxidations under similar conditions. This is in contrast to the behavior of Pt/Al_2O_3, which does not show oxygen evolution and no reducibility at lower temperature. At relatively lower temperatures (below 250 °C), Pt/Al_2O_3 shows almost no activity in benzene oxidation.

4.5. Discussion on the Oxidative Catalytic Mechanism of OMS-2. Manganese oxides have shown excellent activity in many oxidation reactions.[8−15,34,35] In the total oxidation of butane, the activities of OL-1 and OMS-1 are much higher than that of Pt/Al_2O_3.[15] Research reported here suggests that OMS-2 is much more active in total oxidation reactions than OL-1 and OMS-1, as well as Pt/Al_2O_3, under our conditions. There are some common mechanisms regarding oxidation catalysis, with activating species being adsorbed oxygen, gaseous oxygen, and/or lattice oxygen atoms. In this study, the roles of these three types of oxygen species have been explored and elucidated.

The results of normal reaction, reaction without gaseous oxygen, and TPSR all suggest that the active oxidation species for OMS-2 is lattice oxygen, especially the reversibly exchangeable oxygen. In TPSR reaction of benzene in He no oxygen was detected but only CO_2, showing that lattice oxygen reacts with benzene to form CO_2. In reactions of benzene and reactions of CO in oxygen-free streams, the initial reaction rates are equal to those reactions with gaseous oxygen under the same conditions on OMS-2. This excludes the involvement of absorbed oxygen or gaseous oxygen in the activation of benzene or CO; otherwise the initial reaction rate with oxygen should be higher. When the reactant contains no gaseous oxygen and after the catalyst is purged with inert gas for a long time (over 1 h, to remove any adsorbed oxygen species), benzene molecules can be activated and reacted on OMS-2 but not on Pt/Al_2O_3. This confirms that lattice oxygen in OMS-2 is the only source for activating benzene and CO. No gaseous oxygen or adsorbed oxygen species are involved in the activation of VOC's or CO over OMS catalysts. From the oxygen-free reaction results, only about 1% of total lattice oxygen were consumed in room-temperature CO oxidation and about 3% of total lattice oxygen consumed in benzene oxidation at 200 °C; the consumed lattice oxygen can be replenished by exposing the manganese oxide catalysts to gaseous oxygen to almost reversibly recover the structure.

5. Conclusions

For the first time the tunnel porosities close to those of the structural features of OMS-2 and OMS-1 have been identified using CO_2 physisorption experiments in this study. These materials are thermally stable in air even at 650 °C, below which lattice oxygen can be evolved from the framework and recovered without destroying the OMS-2 structure. The surface acidity of OMS-2 as well as OMS-1 and OL-1 has also been studied in detail. Both L and B acid sites have been observed with OMS-2. B acid sites are found to enhance the total oxidation reactions. In addition, OMS-2 has been found to possess excellent hydrophobicity and strong affinity toward organic compounds, capable of selectively adsorbing volatile organic compounds in the presence of water vapor, thus retaining good durability in total oxidation of hydrocarbons where water is formed via oxidation reactions. Reaction experiment results show that the lattice oxygen atoms of manganese oxides are the active species for oxidation of organic species and CO. The gaseous oxygen molecules oxidize the reduced Mn species and recover/maintain the catalytic activity. The physicochemical properties of OMS-2, high porosity, acidity, hydrophobicity, and easy removal of lattice oxygen and recovery, account for the excellent catalytic properties of OMS-2 in oxidation reactions.